THE JOURNAL OF BIOLOGICAL CHEMISTRY VOL. 288, NO. 42, pp. 30626–30635, October 18, 2013

The Nitric-oxide Reductase from *Paracoccus denitrificans* Uses a Single Specific Proton Pathway*

Received for publication, June 26, 2013, and in revised form, September 6, 2013 Published, JBC Papers in Press, September 6, 2013, DOI 10.1074/jbc.M113.497347

Josy ter Beek[1], **Nils Krause**[2], **Joachim Reimann**[3], **Peter Lachmann, and Pia Ädelroth**[4]

From the Department of Biochemistry and Biophysics, The Arrhenius Laboratories for Natural Sciences, Stockholm University, SE-106 91 Stockholm, Sweden

Background: NO reductase (NOR) takes up protons from the opposite side of the membrane compared with other heme-copper oxidases.
Results: NOR is sensitive to mutations along the suggested proton pathway 1 but not the others.
Conclusion: Only pathway 1 is used for proton transfer.
Significance: Although no energy is conserved, proton transfer still occurs through a specific pathway.

The NO reductase from *Paracoccus denitrificans* reduces NO to N_2O ($2NO + 2H^+ + 2e^- \rightarrow N_2O + H_2O$) with electrons donated by periplasmic cytochrome *c* (cytochrome *c*-dependent NO reductase; *c*NOR). *c*NORs are members of the heme-copper oxidase superfamily of integral membrane proteins, comprising the O_2-reducing, proton-pumping respiratory enzymes. In contrast, although NO reduction is as exergonic as O_2 reduction, there are no protons pumped in *c*NOR, and in addition, protons needed for NO reduction are derived from the periplasmic solution (no contribution to the electrochemical gradient is made). *c*NOR thus only needs to transport protons from the periplasm into the active site without the requirement to control the timing of opening and closing (gating) of proton pathways as is needed in a proton pump. Based on the crystal structure of a closely related *c*NOR and molecular dynamics simulations, several proton transfer pathways were suggested, and in principle, these could all be functional. In this work, we show that residues in one of the suggested pathways (denoted pathway 1) are sensitive to site-directed mutation, whereas residues in the other proposed pathways (pathways 2 and 3) could be exchanged without severe effects on turnover activity with either NO or O_2. We further show that electron transfer during single-turnover reduction of O_2 is limited by proton transfer and can thus be used to study alterations in proton transfer rates. The exchange of residues along pathway 1 showed specific slowing of this proton-coupled electron transfer as well as changes in its pH dependence. Our results indicate that only pathway 1 is used to transfer protons in *c*NOR.

Cytochrome *c*-dependent NO reductase (*c*NOR)[5] from *Paracoccus denitrificans* is an integral membrane protein complex that reduces nitric oxide to nitrous oxide ($2NO + 2H^+ + 2e^- \rightarrow N_2O + H_2O$). Nitric oxide reductases (NORs) are mostly found in denitrifying bacteria that stepwise reduce NO_3^- to N_2 gas (via NO_2^-, NO and N_2O). NORs are also expressed in various pathogenic non-denitrifying bacteria in order to inactivate the toxic NO that is produced by the immune system of the host. NORs are members of the heme-copper oxidase (HCuO) superfamily. Most members of this superfamily reduce O_2 to H_2O and conserve the liberated free energy by pumping protons across the membrane, thus maintaining an electrochemical gradient. In addition, electrons are donated from the (positive, lower pH) outside, and protons needed for water formation are taken up strictly from the (negative, higher pH) inside. For this purpose, the O_2-reducing HCuOs use defined proton transfer pathways (one or two) from the cytoplasm into the active site and a route for pumped protons to the outside that is less well defined (for recent reviews on *c*NOR and proton transfer pathways in the HCuO superfamily, see Refs. 1 and 2). *c*NOR, on the other hand, has been shown not to contribute to the electrochemical proton gradient, although the amount of free energy available from NO reduction is similar to that for O_2 reduction (3–5). Electrons are donated by soluble carriers in the periplasm, so for the overall reaction to be non-electrogenic, protons used for NO reduction must also originate in the periplasmic (outside) solution.

*c*NOR is isolated as a complex of two subunits, NorB and NorC (see Fig. 1*A*). NO reduction takes place in the NorB subunit that contains three redox centers: two *b*-type hemes (hemes *b* and b_3) and a non-heme iron (Fe_B). Heme b_3 and the non-heme iron form the binuclear center, where nitric oxide is bound and reduced. NorC is a membrane-anchored cytochrome *c* with one *c*-type heme, which presumably forms the site of electron entry. In addition to NO reduction, *c*NOR can

* This work was supported by grants from the Faculty of Science at Stockholm University and the Swedish Research Council (to P. Ä.).
[1] Supported in part by a grant from the Carl Trygger Foundation and from Stockholm University.
[2] Present address: Experimental Physics: Genetic Biophysics, Freie Universität Berlin, Arnimallee 14, D-14195 Berlin, Germany.
[3] Present address: Dept. of Microbiology, Faculty of Science, Institute of Wetland and Water Research (IWWR), Radboud University of Nijmegen, Nijmegen, The Netherlands.
[4] To whom correspondence should be addressed. Tel.: 46-8-164183; Fax: 46-8-153679; E-mail: piaa@dbb.su.se.

[5] The abbreviations used are: *c*NOR, cytochrome *c*-dependent NO reductase; NOR, NO reductase; HCuO, heme-copper oxidase; DDM, *n*-dodecyl-β-D-maltoside; MD, molecular dynamics; PW, pathway; AH, internal proton donor; ETPT, proton-coupled electron transfer reaction (not intended to indicate the order of the reactions) during the reduction of O_2 by fully reduced *c*NOR.

also catalyze O_2 reduction (6–8). Site-directed mutations that affect NO reduction affect O_2 reduction in a similar manner (7, 9, 10); thus, presumably the same catalytic components are used for both reactions. Furthermore, proton transfer occurs from the same side with similar rates and amplitudes during single-turnover reactions between the fully reduced *c*NOR with NO (11, 12) and O_2 (8).

Recently, the crystal structure of a *c*NOR from *Pseudomonas aeruginosa* (13), highly homologous (52% sequence identity) to *c*NOR from *P. denitrificans*, was determined, and based on this structure and molecular dynamics (MD) simulations, three different proton transfer pathways were proposed, all leading from the periplasmic side of the membrane (see Fig. 1) (13–15).

Proton transfer pathway (PW) 1 was predicted (13, 15) to involve the following residues (*P. aeruginosa* numbering with *P. denitrificans* numbers in parenthesis): Glu-135 (Glu-122), Asp-198 (Asp-185), Lys-53^C (Lys-54^C; the superscript "C" indicates the NorC subunit), and Glu-57^C (Glu-58^C) (see Fig. 1, *A* and *B*, and Table 1). MD simulations supported the formation of a well hydrated, hydrogen-bonded network and indicated that additional residues were involved: Arg-134 (Arg-121), Lys-199 (Lys-186), and Glu-70^C (Glu-71^C) (15). The entrance of the pathway was kept open by rigid hydrogen bonding networks between Glu-57^C, Lys-53^C, Arg-134, and Asp-198 (15).

PW 2 was predicted (13) to go from the heme *c* propionate via Gln-415 (Gln-398), Gln-411 (Gln-394), Gln-340 (Gln-326), Ala-75^C (Ala-76^C), Thr-66^C (Thr-67^C), and Gly-69^C (Gly-70^C) (see Fig. 1, *A* and *C*, and Table 1). Glu-145^C in the *P. aeruginosa* *c*NOR was also predicted to be involved, but the *P. denitrificans* *c*NOR has an Ala at the equivalent position (Ala-149^C). In MD simulations (15), a large hydrophilic region around Gln-415, Glu-77^C, Arg-416, and Thr-66^C was formed that is connected to the bulk solvent. However, the two loops with Gly-340 and Gly-69^C together with the Tyr-73^C (which ligates a Ca^{2+}; see Fig. 1) prevented water from this cavity reaching the water cluster around the heme b_3 propionates further on in the path. Pathway 2 was therefore concluded to be unlikely (15), but it could not be excluded without experimental data.

PW 3, not observed in the crystal structure but suggested from MD simulations (15), is lined by Glu-135 (Glu-122, shared with PW 1), Glu-138 (Glu-125), Arg-57 (Arg-50), Asn-54 (Asn-47), and Asn-60^C. The Asn-60^C is not conserved and is an alanine in *P. denitrificans* (Ala-61^C) (Fig. 1, *A* and *D*, and Table 1). Asn-54 and Asn-60^C were predicted to form a gate that could open and provide connectivity between the bulk water and an internal hydrated cavity.

When studying the role of individual amino acids for proton transfer, the flow-flash technique has provided extensive information about the HCuOs. Here a single turnover of fully reduced enzyme with O_2 is studied time-resolved so that individual transitions can be resolved. We have previously studied the oxidation of the fully reduced *c*NOR by O_2 using this technique and found a transition that involves proton-coupled electron transfer from the hemes *b* and *c* to the active site, modeled as rate-limited by proton transfer from an internal group (*e.g.* amino acid, H_2O molecule, or part of cofactor), crucial for proton transfer to the catalytic site, with a pK_a of 6.6 (8). This transition should thus be specifically sensitive to changes in the rate of proton transfer, and in this work we further demonstrate that it shows a kinetic isotope effect (when H_2O was exchanged for D_2O as the solvent) of ~4 for the maximum rate constant, indicating that the transition is limited by the rate of proton transfer.

Before the crystal structure was known, we had constructed a model of the NorB from *P. denitrificans* based on the homology to structurally defined HCuOs, and a proton pathway was predicted based on this model, sequence conservation, and biochemical studies (5). This pathway involved residues Glu-135 (Glu-122) and Glu-138 (Glu-125) and was supported by data on *P. denitrificans* *c*NOR Glu-122 and Glu-125 variants, which showed effects on catalytic turnover (7, 16) as well as proton-coupled electron transfer (9). The crystal structure of the *c*NOR from *P. aeruginosa* (13) later showed that the Glu-135 is in fact coordinating a Ca^{2+} (see Fig. 1), and the Glu-138 stabilizes the loop in which the Glu-135 is located. These residues, although predicted to line the recently proposed proton transfer pathway 1 (Glu-135) and 3 (Glu-135 and Glu-138), thus have structural roles that make interpretations about their roles in proton transfer difficult.

In this work, based on the pathways proposed from the crystal structure and MD simulations, we exchanged individual residues along each of the three proposed pathways for non-protonatable residues. We chose the residues furthest away from the Ca^{2+}, Fe_B, or hemes, because they are less likely to have structural roles. These variants were characterized in terms of their catalytic turnover with both NO and O_2, their ligand binding properties with CO and O_2, and finally their proton-coupled electron transfer rates and amplitudes. Our results strongly favor pathway 1 as the only functional proton pathway in *c*NOR.

EXPERIMENTAL PROCEDURES

Cloning, Expression, and Purification—The pNOREX plasmid with the *norB* and *norC* genes was used for *c*NOR expression (7). Mutations were introduced directly in pNOREX with the use of the QuikChange XL site-directed mutagenesis kit (Stratagene). Correctly mutated pNOREX was transformed to the *E. coli* JM109 strain together with the pEC86 vector as described (7). *E. coli* was grown, and *c*NOR was expressed and purified essentially as described (9) with a few alterations for the *c*NOR variants and the wild type used for the comparison with the *c*NOR variants (but not for the experiments with wild type in D_2O). The altered purification protocol was as follows. Membrane vesicles from a 6-liter cell culture were solubilized in 100 ml of buffer containing 100 mM Tris, pH 7.6, 50 mM NaCl, and 1% (w/v) *n*-dodecyl-β-D-maltoside (DDM). The solution was incubated at 4 °C with constant stirring for 1 h. Unsolubilized material was removed by centrifugation (30 min, 185,000 × *g*, 4 °C), and the supernatant was filtered over a 0.2-μm filter. The filtrate was diluted twice (with 100 mM Tris, pH 7.6, and 50 mM NaCl) to lower the DDM concentration and loaded at 2 ml/min on a 110-ml Q-Sepharose high performance (GE Healthcare) column pre-equilibrated with the same buffer and 0.05% (w/v) DDM. The column was washed with ~300 ml of 100 mM Tris, 50 mM NaCl, and 0.05% (w/v) DDM at 5 ml/min. *c*NOR was eluted from the column in a 475-ml gradient of 200–500 mM NaCl with 20 mM Tris, pH 7.6, and 0.05% (w/v) DDM at 4 ml/min. 5-ml fractions were collected and diluted 3× in 20 mM

Tris, pH 7.6, and 0.05% (w/v) DDM. The absorbance spectra of the collected fractions were analyzed via a dip probe connected to a Cary 50 Bio spectrophotometer (Varian). Fractions with an $A_{280\ nm}/A_{410\ nm}$ of <2 were collected and concentrated over a 100 kDa cut-off filter (Millipore). 20 mM Tris, pH 7.6, and 0.05% (w/v) DDM were added so that the NaCl concentration was below 50 mM. 25–100-μl fractions of 20–150 μM purified protein ($A_{280\ nm}/A_{410\ nm}$ ~1) were flash frozen in liquid nitrogen and stored at −80 °C.

The presence of correctly inserted *b* and *c* hemes in all the *c*NOR variants was verified via UV-visible spectra from 260 to 700 nm on a Cary 50 or 400 spectrophotometer (Varian). The *c*NOR concentration was calculated from $\epsilon_{550\ nm\ red\text{-}ox} = 70\ mM^{-1}\ cm^{-1}$.

Multiple Turnover—The reduction rates of the *c*NOR variants with O_2 and NO were essentially determined as described in (10), but all measurements were conducted at 30 °C, and NO measurements were done with a specific NO electrode (World Precision Instruments) and recorded via the LabScribe2 software (World Precision Instruments). There were also small differences in the reaction set-up. For the multiple-turnover measurements with NO, NO-saturated water (2 mM NO) was added in five steps of 5 μl (10 μM/addition) to a deoxygenated solution of 50 mM HEPES, pH 7.5, 50 mM KCl, 0.05% (w/v) DDM, 30 mM glucose, 20 units/ml catalase, 1 unit/ml glucose oxidase, 500 μM *N,N,N′,N′*-tetramethyl-*p*-phenylenediamine, and 20 μM cytochrome *c* (horse heart; Sigma-Aldrich). This resulted in five equal steps in the NO signal. Then 3 mM ascorbate was added (this results in some background signal), followed by 25–100 nM *c*NOR. Because of substrate inhibition at high [NO], the obtained maximum rate was calculated from the slope at low [NO] (~5 μM). At this part of the curve, the ascorbate background is negligible (as verified by a measurement without the addition of *c*NOR). O_2 turnover was measured in a solution of 50 mM HEPES, pH 7.5, 50 mM KCl, 0.05% (w/v) DDM, 500 μM *N,N,N′,N′*-tetramethyl-*p*-phenylenediamine, 20 μM cytochrome *c*, and 3 mM ascorbate with a Clark-type electrode (Hansatech). The maximal rate was obtained directly after *c*NOR (at ~250 nM) addition, and the background rate, recorded for ~1 min just before the *c*NOR addition, was subtracted.

Flash Photolysis and Flow-Flash—Samples of ~5 μM *c*NOR were prepared, and measurements were made as described in Ref. 8 on a set-up described in Ref. 17. In short, samples of ~5 μM *c*NOR, 10 mM HEPES, pH 7.5, 50 mM KCl, 0.05% (w/v) DDM, 30 mM glucose, 20 units/ml catalase, 0.2 μM *N*-methylphenazinium methosulfate were prepared in a modified Thunberg cuvette. The sample was made anaerobic with N_2(g), 0.5 unit/ml glucose oxidase was added to remove the remaining oxygen, and 2 mM ascorbate was added to reduce *c*NOR. The reduced sample was put under 100% (v/v) CO(g) and incubated overnight at 4 °C. CO recombination was studied by flash photolysis; the sample was illuminated with a short laser flash (10 ns, 200 mJ, 523 nm, Nd-YAG laser, Quantel), and the kinetic traces were recorded at the indicated wavelength on a digital oscilloscope. The CO concentration was then lowered to ~30% (v/v, 70% N_2(g)) until the average rebinding time constant was ~100 μs. ~50 μM dithionite was added to the *c*NOR sample, and the protein sample was connected to the stopped-flow syringe that was preincubated with 100 mM dithionite and washed with anaerobic water. The other syringe contained an oxygenated buffer with 50 mM HEPES, pH 7.5, 50 mM KCl, and 0.05% (w/v) DDM. To look at pH dependence, the HEPES was exchanged for different buffers at various pH values: MES (pH 6.0–7.0, HEPES (pH 7–8.5), Tris (pH 8.5), and citric acid (pH <6). The protein and the buffer samples were mixed in a 1:5 ratio (protein/oxygenated buffer) in a modified stopped-flow apparatus (Applied Photophysics), and after a 200-ms delay, the laser flash was applied to dissociate CO and allow O_2 to bind and initiate the reaction.

Data Handling and Analysis—The time course of the reaction was studied from microseconds to seconds (via two channels, one recording 10 ms and one channel, prefiltered at 30 kHz, recording 2 s) at different wavelengths in the Soret and α

TABLE 1

Overview of the conservation of residues in predicted proton transfer pathways

Ps. aer., Pseudomonas aeruginosa; Pa. den., Paracoccus denitrificans.

Pathway	*Ps. aer.*	*Pa. den.* [b]	*Suggested role*	Conservation (other a.a.) [a]
1	R134	R121	Proton transfer Hydrogen bond with D198	**96% R** (rest: N, I, M, L)
	E135	**E122**	Ca^{2+} ligand and proton transfer? (9), overlaps with PW 3	88% E (9% K, rest: H, S, V, P)
	D198	**D185**	Proton transfer. Structural role? Hydrogen bonds with R134, $K53^C$	**96% D** (2% E, rest: A, S, Q)
	K199	K186	Proton transfer Hydrogen bond with $E70^C$	72% K (11% Q, 7% E, 6% S, rest: I, T, W, H)
	$K53^C$	**$K54^C$**	Proton transfer Hydrogen bonds with D198, $E57^C$	**100% K**
	$E57^C$	**$E58^C$**	Proton transfer Hydrogen bond with $K53^C$	77% E (18% Q, rest: H, D)
	$E70^C$	$E71^C$	In conserved loop with Ca^{2+} ligands $G71^C$ and $Y73^C$, hydrogen bonds with residues in NorB	80% E (17% N, rest: H, Q, S, F)
2	G340	G326	In sharp turn and interacts with D-ring propionate of heme b_3, blocks proton entry (MD simulations (15))	**99% G (rest: A)**
	Q411	**Q394**	?	**98% Q** (rest: E, D)
	Q415	**Q398**		71% Q (21% E, 6% W, rest: S, V, Y)
	R416	R399	Second shell heme b_3 [c]	**100% R**
	$T66^C$	$T67^C$		84% T (15% S, rest: A)
	$G69^C$	$G70^C$	Sharp turn in conserved loop with Ca^{2+} ligands $G71^C$ and $Y73^C$, blocks proton entry (MD simulations (15))	**100% G**
	$Y73^C$	$Y74^C$	Ca^{2+} ligand, blocks proton entry in MD simulations (15)	**99% Y** (1% R)
	$A75^C$	$A76^C$	In conserved loop with Ca^{2+} ligands $G71^C$ and $Y73^C$, < 4Å from heme *c*	**93% A (7% G)**
	$E77^C$	**$E78^C$**	In conserved loop with Ca^{2+} ligands $G71^C$ and $Y73^C$, forms many hydrogen bonds (see Fig. 1C)	**76% E (24% D)**
	$E145^C$	$A149^C$	Not conserved and therefore unlikely to play a role of interest	40% A, 27% E (rest: S, K, G, L, Q, P, V ,T or -)
3	N54	**N47**		77% N (rest: S, E H, D, M, A)
	R57	R50	Hydrogen bond network: heme *b* propionates and Ca^{2+}	**97% R (rest: K)**
	E135	**E122**	Ca^{2+} ligand and proton transfer? (9), overlaps with PW 1	88% E (9% K, rest: H, S, V, P)
	E138	**E125**	In loop with E122 (Ca^{2+} ligand), hydrogen bonds with R57, T61, N62 in helix II of NorB	**96% E (rest: D)**
	$N60^C$	$A61^C$	Not conserved and therefore unlikely to play a role of interest	52% N (17% H, 13% R, 10% K rest: Y, Q, A)

[a] Percentage conservation was calculated from the alignment in Fig. S5 of Ref. 18, 141 sequences. The value for Glu-77^C ($E77^C$) deviates slightly from the reported conservation in Ref. 18.

[b] The roles of the residues in boldface type have been investigated in this study or in Ref. 9.

[c] Hydrogen bonds with backbone His-339, which hydrogen-bonds with D propionate of heme b_3.

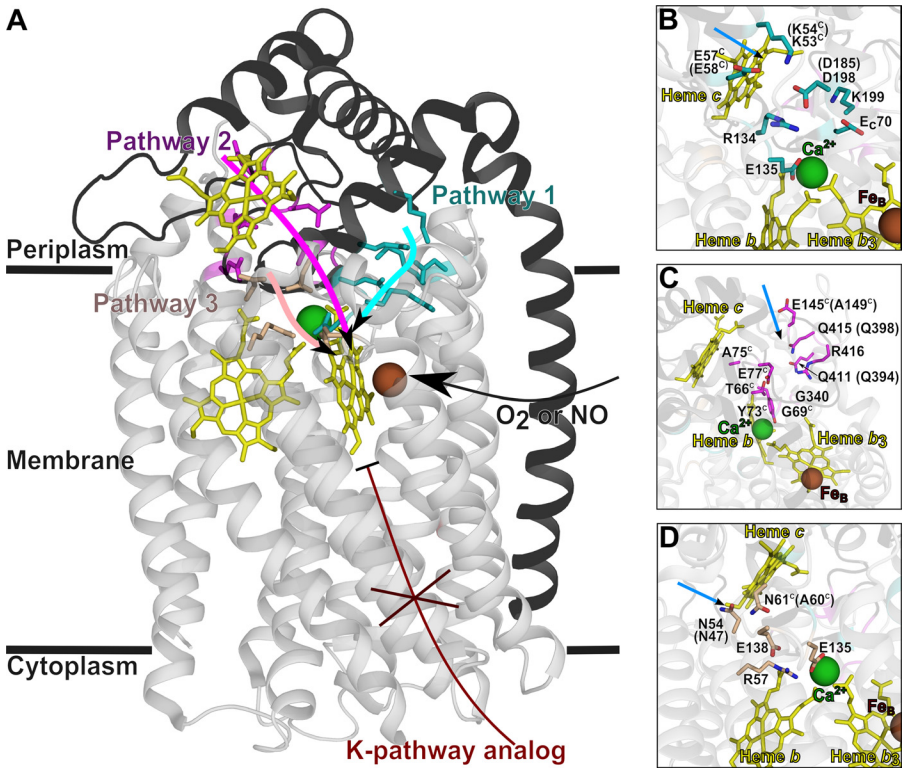

FIGURE 1. **Structure of *c*NOR from *P. aeruginosa* (Protein Data Bank code 3O0R) (13) with the predicted proton transfer pathways.** The NorB (*light gray*, *transparent*) and NorC (*black*, *transparent* in *B–D*) subunits are shown in a *helical representation*. *A*, the residues that are predicted to be involved in proton transfer are indicated with *sticks*, in *cyan* (pathway 1), *magenta* (pathway 2), or *wheat* (pathway 3). The location of the K-pathway (not present in *c*NOR but important in other HCuOs) is indicated in *dark red*. *B–D*, *close-up* of the proton transfer pathways. The *blue arrows* indicate the point of entrance for waters from the bulk. The predicted proton transfer pathways are indicated with *stick representations* in *cyan* (pathway 1; *A*), in *magenta* (pathway 2; *B*), or *wheat* (pathway 3; *C*). The corresponding residues in *P. denitrificans* *c*NOR are indicated in *parenthesis* in case they are different or if they were exchanged in this study. Residues in NorC are indicated with a *C* in *superscript*. This figure was prepared with PyMOL (Schrödinger, LLC, New York).

regions. At each wavelength, 100,000 data points were collected, and the data set was then reduced to ~1000 points by averaging over a progressively increasing number of points. The time-resolved absorbance changes were fitted individually or globally to a model of consecutive irreversible reactions with the software package Pro-K (Applied Photophysics).

The pH dependence of the proton-coupled electron transfer phase was fitted with the following equations (8),

$$k_{obs}(pH) = \alpha_{AH}(pH) \times k_H \quad \text{(Eq. 1)}$$

$$\alpha_{AH}(pH) = \frac{1}{1 + 10^{pH - pK_{AH}}} \quad \text{(Eq. 2)}$$

where k_{obs} represents the obtained rate constant at a certain pH, and k_H is the maximum rate at low pH. k_H is the rate-limiting internal proton transfer (in Ref. 8 presumed to be from a group, AH (assumed to be in rapid equilibrium with bulk pH), to the active site). α_{AH} is the fraction of protonated AH, determined by its pK_a and the pH. For wild type, a small background rate, k_0, was added to Equation 1 (8).

Kinetic Isotope Effect—For the flow-flash experiments in D_2O, H_2O in the solution was exchanged for D_2O (99% (v/v); Cambridge Isotope Laboratories Inc.) by concentration and dilution in 10 mM Tris, 50 mM KCl, 0.05% (w/v) DDM, pH 7, on a 100 kDa cut-off filter (Millipore). The oxygenated buffers were also made with D_2O. The reported pH* values in D_2O are the pH meter readings, not the pD value (which is ~0.4 pH units higher).

RESULTS

Conservation of Residues in the Predicted Proton Transfer Pathways

In Table 1, we have listed the conservation pattern of the residues involved in the three predicted proton transfer pathways (based on the alignment of 141 *c*NOR sequences in Ref. 18). Some, but not all, residues of pathway 1 are highly conserved. There are also some highly conserved residues in pathways 2 and 3, but for most of them, we suggest a role that is not related to proton transfer (Table 1), based on the crystal structure (13).

cNOR Variants Made

In pathway 1, we constructed variants for the two amino acids at the entrance of the pathway: K54A^C (Lys-53^C in *P. aeruginosa*) and E58Q^C (Glu-57^C). We also substituted the following aspartate, Asp-185 (Asp-198), for a glutamate (to maintain the negative charge but change the side chain length), asparagine (to maintain the side chain length but remove the charge), or alanine (for both a drastic change in side chain length and the removal of charge).

In pathway 2, the initial glutamate, Glu-145^C (*P. aeruginosa*; Fig. 1*C*), is an alanine in the *P. denitrificans* *c*NOR

(Table 1). We therefore exchanged the next polar residue in the path, the equivalent of Gln-415, for a hydrophobic leucine (Q398L). We also changed the following glutamine (the equivalent of Gln-411; Fig. 1*C* and Table 1) for a hydrophobic methionine (Q394M).

In pathway 3, Asn-54 and Asn-60^{C} were predicted to form a gate that could open and provide connectivity between the bulk water and an internal hydrated cavity (15). The Asn-60^{C} is not conserved and is an alanine in *P. denitrificans* (Ala-61^{C}) (Fig. 1, *A* and *D*, and Table 1). We constructed *c*NOR variants for the other asparagine: N47F and N47L (Asn-54 in *P. aeruginosa* *c*NOR; Fig. 1*D*). All other PW 3 residues have structural roles (Table 1), and their importance was therefore not analyzed in this study.

TABLE 2

Overview of *c*NOR variants constructed

Ps. aer., Pseudomonas aeruginosa; Pa. den., Paracoccus denitrificans.

Res. in *Ps. aer.* (Pathway)	Mutation in *Pa. den.* (Expr.) [a]	multiple turnover activity (e^-/s) (% of WT activity)		ETPT τ (ms)
		NO [b]	O_2 [c]	
	WT (+++)	8.8 ± 0.2 (100%) [d]	6.1 ± 2.9 (100%)	20 [e]
K53^{C} (1)	K54A^{C} (+++)	1.5 ± 0.1 (17%)	1.8 ± 0.6 (30%)	250
E57^{C} (1)	E58Q^{C} (+++)	0.7 ± 0.0 (8%)	1.3 ± 0.6 (21%)	500
D198 (1)	D185E (+++)	1.0 ± 0.1 (11%)	1.0 ± 0.9 (16%)	-
	D185N (+)	<< 1.0 (<<11%)	0.7 ± 0.3 (11%)	-
	D185A (+)	0 (0%)	0 (0%)	-
E77^{C} (2)	E78F^{C} (-)	This mutant could not be tested since it did not express		
Q411 (2)	Q394M (+++)	5.9 ± 0.2 (67%)	2.0 ± 0.4 (33%)	20
Q415 (2)	Q398L (+++)	8.6 ± 0.4 (98%)	3.7 ± 1.1 (61%)	20
N54 (3)	N47F (+++)	10.1 ±0.8 (115%)	6.0 ± 2.4 (98%)	25
	N47L (++)	Altered optical spectra and CO binding, not evaluated further		

[a] Expression (Expr.) indicated as +++ for WT-like levels of *c*NOR.
[b] The error indicates the range for two measurements for NO multiple turnover.
[c] S.D. value is indicated for O_2 multiple turnover for 5–7 measurements.
[d] The NO multiple turnover activity of the wild type was lower than reported previously (7, 10), possibly because of slight alterations in the purification protocol. The *c*NOR variants were prepared in the same way as the wild type, such that the percentage activity reports a valid comparison.
[e] ETPT stands for the proton-coupled electron transfer during single-turnover O_2 reduction. The ETPT in wild type was slightly faster than before (25 ms in Ref. 8).

Expression, Optical Spectra, and Multiple Turnover

Most *c*NOR variants along the three proposed pathways could be expressed and resulted in stable protein complexes, except for E78F^{C} (in pathway 2; Table 2). The stable *c*NOR variants were characterized with respect to their optical spectra (oxidized and reduced) and their catalytic turnover rates with NO and O_2. All variants showed wild type-like optical spectra (except for N47L, which was therefore not studied further), showing that hemes *b* and *c* were integrated normally into the *c*NOR. All *c*NOR variants with mutations in pathway 1 were significantly affected in the ability to reduce NO and O_2 (Table 2), although the mutations were >7 Å away from both the active site and the Ca^{2+}. The expressed and stable *c*NOR variants with mutations in pathway 2 (Q394M and Q398L) or pathway 3 (N47F) reduced both NO and O_2 with rates that were more similar to wild type (Table 2). N47F showed wild type rates for both NO and O_2 reduction. Q398L reduced NO as wild type but had a slightly slower rate with O_2 (~61%). Q394M reduced NO at ~67% and O_2 at ~33% of the wild type rate.

Single-turnover O_2 Reduction

Multiple-turnover rates cannot be used to discriminate between changes in proton transfer rates and any other change in the reaction cycle. Therefore, we studied the transitions as the fully reduced *c*NOR is oxidized by O_2. In this reaction for wild type (WT) *c*NOR, O_2 binds to heme b_3 with a time constant of ~50 μs at 1 mM O_2 (k_{obs} ~2×10^4 s^{-1}), followed by proton-coupled electron transfer from the hemes *b* and *c* to the active site with a time constant of ~20 ms at pH 7.5 (k_{obs} ~60 s^{-1}; Figs. 2 and 3 and Table 2). These time constants deviate slightly from the ~40 μs for O_2 binding and ~25 ms for the second phase as reported previously (8), probably because of the slightly altered purification conditions. Based on its pH dependence (Fig. 2*B*), the 20–25-ms phase was modeled to be rate-limited by proton transfer from an internal group with a pK_a of 6.6 (see Ref. 8 and Equations 1 and 2). In this paper, we

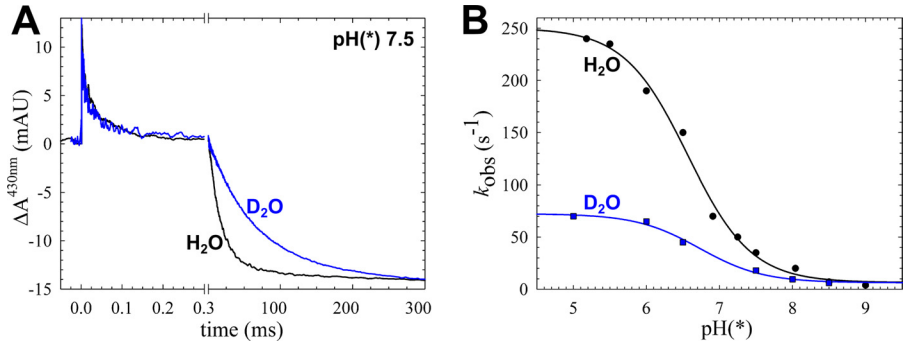

FIGURE 2. **The kinetic (deuterium) isotope effect on ETPT during the reaction between fully reduced *c*NOR and O_2.** *A*, trace obtained at 430 nm of wild type *c*NOR in H_2O or D_2O at pH(*) 7.5, showing the change in absorbance (Δ*A*) over time (with the laser flash set at $t = 0$). The data were normalized to the CO_{off} step at $t = 0$ for the rapid time scale and to the amplitude of the ETPT (which varies slightly between experiments) for the longer time scale. The laser artifact at $t = 0$ has been removed for clarity. The CO_{off} reaction results in a rapid increase of absorbance, and O_2 binding (with τ of ~40–50 μs) then results in a decrease. On the longer time scale, the ETPT is seen as a further negative Δ*A* (τ of ~20–25 ms in H_2O). *B*, the rate of the ETPT in D_2O (*blue*) and H_2O (*black*) as a function of pH(*). The D_2O data were fitted to a pK_a* of 6.7 ± 0.1 and a k_H (maximal rate at low pH) of 66 ± 3 s^{-1}, and the H_2O data (which are from Ref. 8) were fitted to a pK_a of 6.6 ± 0.1 and a k_H of 244 ± 7 s^{-1}. *mAU*, milliabsorbance units.

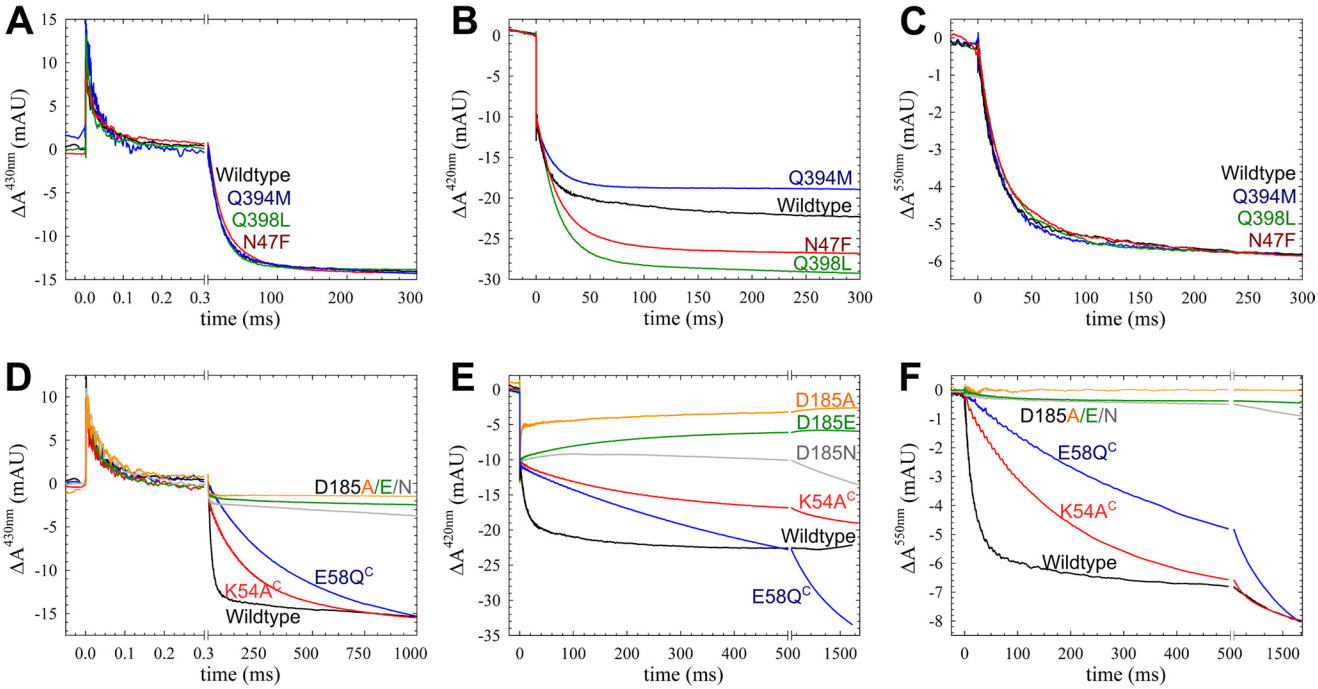

FIGURE 3. **The reaction between fully reduced *c*NOR variants and O_2.** The traces show the change in absorbance (ΔA) over time (with the laser flash set at $t = 0$) for *c*NOR wild type and the constructed variants. *A–C*, variants in proton transfer PW 2 and 3; *D–F*, variants in PW 1. Data were recorded at 430 nm (*A* and *D*), 420 nm (*B* and *E*), and 550 nm (*C* and *F*). The laser artifact at $t = 0$ has been removed for clarity. At 420 nm, the CO_{off} results in a rapid decrease in absorbance on the fast time scale, and the subsequent oxidation of the hemes (ETPT) results in a further slower negative ΔA. The amplitude of the ETPT varied slightly between experiments for both WT and variants and was normalized at 550 nm (reporting on the heme *c*) and 430 nm to the same ΔA for easier comparison of the rates. For the 420 nm trace and the shorter time scale at 430 nm, the CO_{off} step was used for normalization. The ΔA in the Asp-185 variants are only normalized to the CO_{off} step, because their ETPT ΔA values deviate from WT much more than the variation between measurements. *A–C*, WT (*black trace*), Q394M (*blue trace*), Q398L (*green trace*), and N47F (*red trace*). Gln-384 and Gln-398 are located in PW 2, and Asn-47 is in PW 3. *D–F*, wild type (*black trace*), E58Q^C (*blue trace*), K54A^C (*red trace*), D185E (*green trace*), D185N (*gray trace*), and D185A (*yellow trace*). *mAU*, milliabsorbance units.

will refer to this phase as the proton-coupled electron transfer (ETPT), but we would like to stress that this term is not intended to imply the order of the reactions.

Kinetic Isotope Effect

To further investigate if the ETPT is indeed limited by proton transfer, we studied its kinetic (deuterium) isotope effect at various pH/pH* values (*i.e.* reporting the pH meter reading for both H_2O and D_2O solutions). The obtained rate constants are plotted in Fig. 2*B*. The observed rate constants in H_2O were previously fitted to a pK_a of 6.6 ± 0.1 and a k_H of 244 ± 7 s^{-1} (8). In D_2O, the corresponding values were pK_a* = 6.7 ± 0.1 and k_{H^*} = 66 ± 3 s^{-1}. The maximum rate constant k_H thus has a kinetic isotope effect (ratio of rate constants in H_2O and D_2O) of 3.7, indicating that this phase is indeed limited by proton transfer (*e.g.* see Ref. 19). The small change in pK_a when exchanging H_2O for D_2O follows the empirical formula (pK_H = 0.929 × pK_{H^*} + 0.42) determined in Ref. 20.

CO and O_2 Binding Rates

In order to further probe the integrity of the active site in our *c*NOR variants, we determined the time constant for CO and O_2 binding. O_2 binding was found to be the same as in wild type, with τ ranging from ~40 to ~50 μs (Fig. 3). Only the D185N and D185A had slightly slower O_2 binding with a τ of ~60 or ~65 μs, respectively (Fig. 3). CO binding in the D185A and the D185E variants was slower than in wild type, whereas it was essentially unchanged for any of the other variants with normal optical spectra (data not shown). The changes in O_2 and/or CO binding in the Asp-185 variants could indicate an altered environment of the b_3 heme. D185N and D185A were also less well expressed (Table 2), indicating that the Asp-185 is needed to produce/maintain a stable and functional *c*NOR.

Proton-coupled Electron Transfer

Because we established that the ETPT is indeed limited by proton transfer, we used it to indicate whether proton transfer was affected in the *c*NOR variants.

Pathways 2 and 3—The pathway 2 substitutions Q398L and Q394M (Gln-415 and Gln-411 in *P. aeruginosa* *c*NOR) had no effect on the ETPT rate (Fig. 3 and Table 2). Also in the N47F *c*NOR variant (Asn-54 in *P. aeruginosa* *c*NOR, PW 3), the ETPT rate was similar to WT (Fig. 3 and Table 2).

Pathway 1—For the Asp-185 (Asp-198 in *P. aeruginosa* *c*NOR) variants, the amplitude for the ETPT is small (430 and 550 nm) or even absent (420 nm), indicating that the reaction is completely inhibited. In the E58Q^C (Glu-57^C in *P. aeruginosa* *c*NOR) variant, the ETPT rate constant is ~30 times slower than in WT at pH 7.5 (with a k_{obs} of ~2 s^{-1}, τ of ~500 ms). The K54A^C (Lys-53^C in *P. aeruginosa* *c*NOR) has an ETPT rate constant that is ~10 times slower (with a k_{obs} of ~4 s^{-1} and τ of ~250 ms) than in WT at pH 7.5.

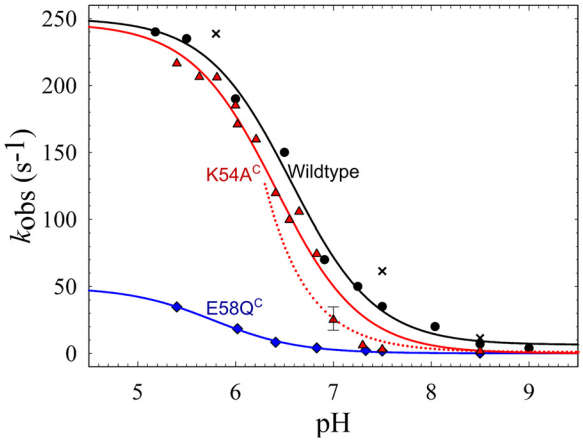

FIGURE 4. **The pH dependence of the ETPT in *c*NOR wild type and variants.** The rates of the ETPT for *c*NOR wild type and the constructed variants that were affected at pH 7.5 are plotted as a function of pH: wild type (*black*; *circles* for the data from Ref. 8 and *crosses* for the data with the slightly altered purification protocol), K54A^C (*red triangles*), E58Q^C (*blue diamonds*). The WT data (from Ref. 8) were fitted to a pK_a of 6.61 ± 0.05 and a k_H of 244 ± 7 s^{-1} (*black line*); K54A^C data were fitted to a pK_a = 6.4 ± 0.1 and a k_H = 247 ± 11 s^{-1} (*red line*); and E58Q^C data were fitted to a pK_a = 5.8 ± 0.1 and a k_H = 49 ± 2 s^{-1} (*blue line*). However, data points for K54A^C did not follow the fit around pH 7–7.5, possibly because the one-exponential fit is an oversimplification for this mutant. As a comparison, also plotted (as a *dotted red line*) is the diffusion rate, assuming k_{diff} of ~2 × 10^8 M^{-1} s^{-1} (see "Results" for details). The *error bar* at pH 7.0 for K54A^C indicates that at this pH the range of possible fits is rather large.

pH Dependence of the Proton-coupled Electron Transfer in Affected cNOR Variants

For the *c*NOR variants that had slower ETPT rate constants at pH 7.5, we further investigated this reaction at various pH values. However, this could not be done for the Asp-185 variants because their ETPT is small or even absent (and the rates can therefore not be fitted).

In the *c*NOR variant E58Q^C, the reaction displayed severely slower rates in the entire pH range that we tested, with a k_H (maximum rate constant) of ~50 s^{-1} (*i.e.* ~5 times slower than for WT) (Fig. 4). The pK_a in E58Q^C shifted from 6.6 to ~5.8.

The K54A^C *c*NOR variant, however, has a similar k_H as wild type (~250 s^{-1}), but the pK_a is shifted from 6.6 to 6.4. The ETPT rate constant in the K54A^C variant was fitted to a single exponential at all pH values for comparison with wild type, although the fit was better with two exponentials at pH values from 6.5 to 7.5. This could explain why the obtained rate constants at pH 7–7.5 were not fitted well to a single pK_a transition (Fig. 4). This behavior can be explained by a model in which at high pH the assumption that the internal protonatable group (AH, Equations 1 and 2) is in rapid equilibrium with the bulk pH is not valid for this *c*NOR variant (because the entry point to the pathway is altered). Thus, at higher pH, proton diffusion to AH becomes rate-limiting, and this proton diffusion rate (tentatively fitted to ~2 × 10^8 M^{-1} s^{-1}) is plotted as a *red dotted line* in Fig. 4. A small background rate k_0 of ~1 s^{-1} was added to this fit. This altered model could also explain the biphasic nature of the ETPT in this *c*NOR variant because in the enzyme population with AH protonated (and not in rapid equilibrium with bulk pH), ETPT can occur with the maximum rate k_H. With a forced one-exponential fit, we would see an average of the two rate constants (k_H and the diffusion-limited rate constant) in the pH range where both populations (protonated/deprotonated AH) contribute significantly. However, we did not pursue a full biphasic fit of the data because of the small number of points that could not be fitted reasonably well with one exponential.

DISCUSSION

The multiple-turnover data with NO and O_2 show severe effects for variants with pathway 1, but not pathway 2 (Q398L, Q394M) or 3 (N47F), residues modified (Table 2). Furthermore, all *c*NOR variants that are affected in their NO turnover are also affected in their O_2 turnover (Table 2). The correlation between O_2 and NO turnover has been observed before (although the extent of the change can differ (7, 10)) and shows the validity of using O_2 as an alternative substrate.

The ET reaction (in this paper called ETPT) during single-turnover reduction of O_2 by fully reduced *c*NOR was previously suggested to be rate-limited by proton transfer based on the uptake of protons from solution with the same rate constant and the pH dependence of the reaction (8). In this work, we show that the k_{max} (k_H) is decreased, from ~250 s^{-1} to ~70 s^{-1} (*i.e.* by a factor of ~4) in D_2O (Fig. 2), which indicates that the rate of proton transfer indeed limits the overall rate constant for this reaction. We thus have strengthened the basis for using this ETPT as a "reporter" for effects on proton transfer rates in *c*NOR. The kinetic isotope effect is higher in A-type HCuOs (the F → O transition has a kinetic isotope effect of 7 (21)), where there are conformational changes needed in the proton pumping process. In *c*NOR we do not expect large conformational changes, because *c*NOR does not pump protons, and no "gating" is required.

The effects on the ETPT in the *c*NOR variants studied here were qualitatively in agreement with the multiple-turnover data, except for Q394M (PW 2), where the turnover rate with O_2 is slower than wild type, whereas the ETPT is unaffected. Presumably, rereduction is slowed in this *c*NOR variant but for reasons unknown at this point. We note, however, that Gln-394 is a highly conserved residue (Table 1). For the other variants in PWs 2 and 3 (Fig. 1), there are no effects on the ETPT (Fig. 3 and Table 2) and no (large) effects on multiple turnover. It could be argued that very few variants were made in PWs 2 and 3, but because we aimed at residues away from the Ca^{2+} and the hemes without other roles, as suggested by the structure (Table 1), few residues were good candidates (especially for PW 3, which shares parts with PW 1). Even so, the reason why the *c*NOR variant E78F^C (in PW 2) was not expressed and N47L (in PW 3) had altered spectra and CO binding properties is possibly because of their close proximity to heme *c* (4.9 and 3.5 Å for Glu-78^C and Asn-47, respectively). Both suggested PWs 2 and 3 in the *P. aeruginosa* *c*NOR contain one residue that is not conserved in *P. denitrificans* *c*NOR (as in many other *c*NORs; see Table 1 and Ref. 18), also indicating that PWs 2 and 3 are not used for proton transfer.

The variants in PW 1 all affect catalytic turnover (Table 2) and the rate of the ETPT (Fig. 3). None of the modified residues have obvious structural roles as, for example, Ca^{2+} ligands (Table 1), and all are >7.5 Å away from the redox centers and the Ca^{2+} site. Therefore, it is unlikely that all of these residues have structural roles and/or control the heme potentials. The

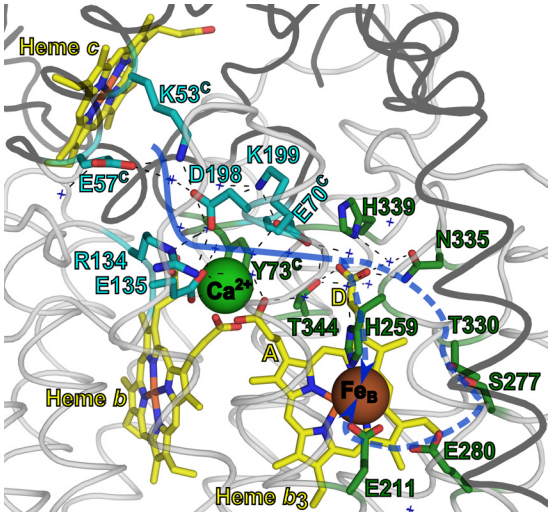

FIGURE 5. **The proton transfer pathway in *c*NOR as indicated in this work.** The structure is the same as in Fig. 1 (*c*NOR from *P. aeruginosa* (Protein Data Bank code 3O0R) (13)) and rendered in the same way (except that for clarity a loop instead of helical representation is used) with the residues in the start of pathway 1 indicated with *sticks* in *cyan* (pathway 1) and the ones predicted to be involved in the continuation of the proton pathway to the active site in *green*. The suggested pathway is indicated with a *blue* (*dotted*) *arrow*. Crystallographic waters in or around the pathway are indicated with *blue crosses*. The *black dotted lines* indicate hydrogen bonds. The *yellow A* and *D* indicate the heme b_3 propionate A and D, respectively.

variants where the Asn-185 (Asn-198 in *P. aeruginosa* *c*NOR) was exchanged for a non-protonatable residue (D185A and D185N) retain some residual activity in multiple turnover. In the single-turnover reaction with O_2, however, only O_2 binding is observed, and there is no ETPT (Fig. 3). This might be due to a limited "window" in which the ETPT reaction can be observed, because on the longer time scale at 420 nm (Fig. 3*E*), a phase that we attribute to CO rebinding is observed, presumably due to a slow re-equilibration between CO and the O_2 at the active site (9, 10). Although D185E had higher multiple-turnover rates than D185A and D185N, its rates were still much lower than those of wild type. The effects on the ETPT seemed too severe for the residue to have a "simple" role in proton transfer because an Asp is only a methyl group shorter than a Glu. The chain length might, however, influence the pathway because the Asp-198 could form hydrogen bonds with Lys-53^C (Lys-54^C), Arg-134 (Arg-121), and various waters (15) (Fig. 5). An alternative explanation is that the aspartate has a more structural role, because the D185N and D185A variants were only expressed at low levels, and ligand binding was also slowed in these variants.

The K54A *c*NOR variant reaches the same maximum rate at low pH, but it has a shifted pK_a and is ~10 times slower than wild type at pH 7.5. Thus, the Lys-54^C (Lys-53^C in *P. aeruginosa*) is important to support rapid proton transfer at the growth pH used for denitrifying conditions (pH 7.5 (22)), where the full denitrification chain is active (23).

In the E58Q^C variant (Glu-57^C in *P. aeruginosa*), even at low pH, the rate constant of the ETPT is still ~5 times slower than in WT, and the pH dependence was fitted with a tentative pK_a of ~5.8. There is thus a severe slowing of the proton transfer rate constants at all pH values, making the effect much more drastic than in K54A^C. The Glu-58^C seems thus to be a very important part of the pathway, presumably forming its entry point (Fig. 5). We note that the Lys-54^C is actually more conserved than the Glu-58^C (100% compared with 77%; Table 1 and Ref. 18). Although we do not have an explanation for this at the moment, we do note that the sequences that do not have Glu-58^C cluster together in the alignment and belong to different subgroups of the *c*NOR family than the subgroup of *P. aeruginosa* and *P. denitrificans* (18). The replacing residues are hydrophilic (Gln, His, or Asp), and there are charged residues in the flanking sequence (3 or less residues away) that might take over the role of the Glu-58^C in these *c*NORs.

The identity of the internal proton donor (AH in Equations 1 and 2, pK_a = 6.6 in wild type) remains unknown. There was a large pK_a shift (>3 pH units upshifted) in the ETPT observed in variants with an exchanged Ca^{2+} ligand (Glu-122 in *P. denitrificans* *c*NOR, Glu-135 in *P. aeruginosa*, also in PW 1) (9). This shift was much larger than the pK_a shifts observed with the variants studied in this work and indicates that the donor is located in the vicinity of the Glu-135. However, the coordination of the Ca^{2+} with multiple groups (one propionate each from the *b* and b_3 hemes, Tyr-73^C, Gly-71^C, and an H_2O) gives many possibilities. Because these residues all have structural roles as Ca^{2+} ligands, it is difficult to study any additional roles. We rule out the Arg-134 (Arg-121 in *P. denitrificans*) as AH, although it is very close and highly conserved (Fig. 1*B* and Table 1) because arginines have been shown to keep their high pK_a values (~12.5) even when embedded in protein interiors (24). The heme *b* propionate and the A propionate of heme b_3 are possible candidates for AH, because one of them could, in principle, transiently dissociate from the Ca^{2+} and be protonated (Fig. 5). The Asp-198 (Asp-185 in *P. denitrificans*) is also a possible candidate, being ~10 Å from the Glu-135, hydrogen-bonded to the Lys-53^C, and giving such severe effects of mutation. However the pK_a shift in the variant of the Lys-53^C equivalent (K54A^C) seems too modest (only 0.2 units) for a residue directly hydrogen-bonded to the proton donor. Although not in direct contact with the Glu-135 or the Ca^{2+}, the D propionate of heme b_3 (Fig. 5) seems like a better candidate for the proton donor for several reasons. First, precisely because it is not coordinated to Ca^{2+}, it could adopt a higher pK_a, possibly around 6.6, and it could still be affected by a change in ligation of the other propionate. Second, the D propionate is better positioned in the path to form a connection "onward" (Fig. 5), toward the reaction intermediate bound at (or between) the irons of heme b_3 and Fe_B. MD simulations (15) postulated that protons could move 1) directly from the water cluster around the A and D propionates of heme b_3 to a water cluster around the active site, 2) from the D propionate of heme b_3 via the His-259 to the active site, or 3) from the D propionate of heme b_3 via Thr-330, Ser-277, Glu-280, and Glu-211 to the active site (Fig. 5). It is tempting to suggest that the proton donor in *c*NOR in the path from the periplasm to the active site became (or originated from, depending on the rooting of the evolutionary tree; see, for example, Ref. 25) the site for extrusion of pumped protons in the O_2-reducing HCuOs, the so-called proton loading site. The A propionate has recently been suggested by several research groups (*e.g.* see Refs. 26 and 27) to be this proton-loading site in O_2-reducing HCuOs (A-, B-, and

C-type, where it should be noted that the location of the A propionate of the active site heme corresponds to the location of the D propionate of the b_3 heme in *c*NOR). Pathway 1 in *c*NOR is not conserved to the closest O_2-reducing HCuO, the C-type, where instead parts of the PW 3 are conserved (15). However, the PW 3 residues conserved to C-type HCuOs (Glu-135 (also involved in PW 1), Glu-138, and Arg-57 in *P. aeruginosa c*NOR) all are involved in defining the Ca^{2+} site (Table 1). This could explain why they are conserved to C-type HCuOs, which have a Ca^{2+} bound in a similar manner (28).

Taken together, our data presented here strongly suggest that *c*NORs, at least the one from *P. denitrificans*, do use a specific pathway for proton transfer from the periplasm into the active site and that this is the suggested pathway 1 (Figs. 1 and 5) and that the other suggested pathways cannot take over the role of pathway 1. We note that a different study, where several residues were mutated in the *c*NOR from *Thermus thermophilus* (18), reached the conclusion that there is no preferred pathway in (this) *c*NOR. They did not investigate PW 3, but they observed effects on turnover rates when changing the residue at the entrance of PW 2, D209E/N/L^C, which is an alanine in *P. denitrificans* (Ala-149^C) and a glutamate in *P. aeruginosa* (Glu-145^C). Their results also differed for residues along pathway 1. Mutating the equivalent of Asp-198 (*P. aeruginosa* numbering) of PW 1 in the *T. thermophilus c*NOR to either Glu or Asn had no effect on turnover (although, when changed into a leucine, the *c*NOR was not assembled). The Glu-57^C is a Gln in *T. thermophilus c*NOR. Lys-53^C is present in *T. thermophilus c*NOR, but its role was not investigated. The reason for the differences between the results of our study and the study with *T. thermophilus c*NOR (18) is not known. It is possible that PW 1 is used in the *P. denitrificans c*NOR (and *P. aeruginosa c*NOR) but not in *T. thermophilus c*NOR. The *P. aeruginosa c*NOR and the *P. denitrificans c*NORs are much more closely related to each other (51% identity between the NorB subunits, both belonging to the Proteobacteria phylum) than to the only distantly related *T. thermophilus c*NOR (belonging to the Thermus phylum and with 38% identity in NorB to both *P. aeruginosa* and *P. denitrificans*). There might be larger differences in the proton transfer pathways between subfamilies in *c*NOR compared with the O_2-reducing HCuOs because no gating is necessary. It is also possible that effects on the proton transfer rates that we see in the *P. denitrificans c*NOR for D185N/D185E would not have been observed in the multiple-turnover experiments with NO in *T. thermophilus c*NOR, given that the overall turnover rate is orders of magnitude lower in the *T. thermophilus* enzyme ($\sim$0.1 s^{-1} compared with $\sim$10 s^{-1} for the *P. denitrificans c*NOR used in this study; Table 2).

In principle, *c*NOR would not need to provide a specific pathway for protons, it could have protons "leak" into the active site from multiple routes. However, the use of a single, specific route can have different reasons. One is the evolutionary relationship to the other heme-copper oxidases. If *c*NOR evolved from an O_2-reducing HCuO that had a specific path for the extrusion of the pumped protons, then this pathway could have been "reversed" in *c*NOR. Also, there is an energetic cost in terms of protein stability involved in creating a polar, water-filled pathway capable of proton transfer in an otherwise hydrophobic protein interior. This might minimize the number of proton transfer pathways to those that are absolutely necessary for function.

Acknowledgments—Dr. Nicholas Watmough (University of East Anglia) is acknowledged for sending the plasmids pNOREX and the pNORXX16 (used originally for mutagenesis, not described here). We thank Liesa Westner for making the first mutants (not described here) in the larger pNOREX plasmid. Anne Roehrig is acknowledged for making the first Asp-185 mutant in the pNORXX16 (not described here). We thank Lina Salomonsson for help with supervising N. K.

REFERENCES

1. Shiro, Y. (2012) Structure and function of bacterial nitric oxide reductases. Nitric oxide reductase, anaerobic enzymes. *Biochim. Biophys. Acta* **1817,** 1907–1913
2. Lee, H. J., Reimann, J., Huang, Y., and Ädelroth, P. (2012) Functional proton transfer pathways in the heme-copper oxidase superfamily. *Biochim. Biophys. Acta* **1817,** 537–544
3. Bell, L. C., Richardson, D. J., and Ferguson, S. J. (1992) Identification of nitric oxide reductase activity in *Rhodobacter capsulatus*. The electron transport pathway can either use or bypass both cytochrome c2 and the cytochrome bc1 complex. *J. Gen. Microbiol.* **138,** 437–443
4. Shapleigh, J. P., and Payne, W. J. (1985) Nitric oxide-dependent proton translocation in various denitrifiers. *J. Bacteriol.* **163,** 837–840
5. Reimann, J., Flock, U., Lepp, H., Honigmann, A., and Ädelroth, P. (2007) A pathway for protons in nitric oxide reductase from *Paracoccus denitrificans*. *Biochim. Biophys. Acta* **1767,** 362–373
6. Fujiwara, T., and Fukumori, Y. (1996) Cytochrome *cb*-type nitric oxide reductase with cytochrome c oxidase activity from *Paracoccus denitrificans* ATCC 35512. *J. Bacteriol.* **178,** 1866–1871
7. Butland, G., Spiro, S., Watmough, N. J., and Richardson, D. J. (2001) Two conserved glutamates in the bacterial nitric oxide reductase are essential for activity but not assembly of the enzyme. *J. Bacteriol.* **183,** 189–199
8. Flock, U., Watmough, N. J., and Ädelroth, P. (2005) Electron/proton coupling in bacterial nitric oxide reductase during reduction of oxygen. *Biochemistry* **44,** 10711–10719
9. Flock, U., Thorndycroft, F. H., Matorin, A. D., Richardson, D. J., Watmough, N. J., and Ädelroth, P. (2008) Defining the proton entry point in the bacterial respiratory nitric-oxide reductase. *J. Biol. Chem.* **283,** 3839–3845
10. Flock, U., Lachmann, P., Reimann, J., Watmough, N. J., and Ädelroth, P. (2009) Exploring the terminal region of the proton pathway in the bacterial nitric oxide reductase. *J. Inorg. Biochem.* **103,** 845–850
11. Hendriks, J. H., Jasaitis, A., Saraste, M., and Verkhovsky, M. I. (2002) Proton and electron pathways in the bacterial nitric oxide reductase. *Biochemistry* **41,** 2331–2340
12. Lachmann, P., Huang, Y., Reimann, J., Flock, U., and Ädelroth, P. (2010) Substrate control of internal electron transfer in bacterial nitric-oxide reductase. *J. Biol. Chem.* **285,** 25531–25537
13. Hino, T., Matsumoto, Y., Nagano, S., Sugimoto, H., Fukumori, Y., Murata, T., Iwata, S., and Shiro, Y. (2010) Structural basis of biological N_2O generation by bacterial nitric oxide reductase. *Science* **330,** 1666–1670
14. Shiro, Y., Sugimoto, H., Tosha, T., Nagano, S., and Hino, T. (2012) Structural basis for nitrous oxide generation by bacterial nitric oxide reductases. *Philos. Trans. R. Soc. Lond. B Biol. Sci.* **367,** 1195–1203
15. Pisliakov, A. V., Hino, T., Shiro, Y., and Sugita, Y. (2012) Molecular dynamics simulations reveal proton transfer pathways in cytochrome *c*-dependent nitric oxide reductase. *PLoS Comput. Biol.* **8,** e1002674
16. Thorndycroft, F. H., Butland, G., Richardson, D. J., and Watmough, N. J. (2007) A new assay for nitric oxide reductase reveals two conserved glutamate residues form the entrance to a proton-conducting channel in the bacterial enzyme. *Biochem. J.* **401,** 111–119
17. Brändén, M., Sigurdson, H., Namslauer, A., Gennis, R. B., Ädelroth, P., and Brzezinski, P. (2001) On the role of the K-proton transfer pathway in

cytochrome *c* oxidase. *Proc. Natl. Acad. Sci. U.S.A.* **98,** 5013–5018
18. Schurig-Briccio, L. A., Venkatakrishnan, P., Hemp, J., Bricio, C., Berenguer, J., and Gennis, R. B. (2013) Characterization of the nitric oxide reductase from *Thermus thermophilus*. *Proc. Natl. Acad. Sci. U.S.A.* **110,** 12613–12618
19. Krishtalik, L. I. (2000) The mechanism of the proton transfer. An outline. *Biochim. Biophys. Acta* **1458,** 6–27
20. Krezel, A., and Bal, W. (2004) A formula for correlating pK_a values determined in D_2O and H_2O. *J. Inorg. Biochem.* **98,** 161–166
21. Karpefors, M., Ädelroth, P., and Brzezinski, P. (2000) Localized control of proton transfer through the D-pathway in cytochrome *c* oxidase. Application of the proton-inventory technique. *Biochemistry* **39,** 6850–6856
22. Harms, N., de Vries, G. E., Maurer, K., Veltkamp, E., and Stouthamer, A. H. (1985) Isolation and characterization of *Paracoccus denitrificans* mutants with defects in the metabolism of one-carbon compounds. *J. Bacteriol.* **164,** 1064–1070
23. Bergaust, L., Mao, Y., Bakken, L. R., and Frostegård, A. (2010) Denitrification response patterns during the transition to anoxic respiration and posttranscriptional effects of suboptimal pH on nitrous [corrected] oxide reductase in *Paracoccus denitrificans*. *Appl. Environ. Microbiol.* **76,** 6387–6396
24. Harms, M. J., Schlessman, J. L., Sue, G. R., and García-Moreno, B. (2011) Arginine residues at internal positions in a protein are always charged. *Proc. Natl. Acad. Sci. U.S.A.* **108,** 18954–18959
25. Gribaldo, S., Talla, E., and Brochier-Armanet, C. (2009) Evolution of the haem copper oxidases superfamily. A rooting tale. *Trends Biochem. Sci.* **34,** 375–381
26. Kaila, V. R., Sharma, V., and Wikström, M. (2011) The identity of the transient proton loading site of the proton-pumping mechanism of cytochrome *c* oxidase. *Biochim. Biophys. Acta* **1807,** 80–84
27. Chang, H. Y., Choi, S. K., Vakkasoglu, A. S., Chen, Y., Hemp, J., Fee, J. A., and Gennis, R. B. (2012) Exploring the proton pump and exit pathway for pumped protons in cytochrome ba3 from *Thermus thermophilus*. *Proc. Natl. Acad. Sci. U.S.A.* **109,** 5259–5264
28. Buschmann, S., Warkentin, E., Xie, H., Langer, J. D., Ermler, U., and Michel, H. (2010) The structure of cbb_3 cytochrome oxidase provides insights into proton pumping. *Science* **329,** 327–330